European Journal of Medicinal Chemistry 90 (2015) 241–250

Contents lists available at ScienceDirect

European Journal of Medicinal Chemistry

journal homepage: http://www.elsevier.com/locate/ejmech

Original article

Novel fatty acid binding protein 4 (FABP4) inhibitors: Virtual screening, synthesis and crystal structure determination

Haiyan Cai [a, b, 1], Qiufeng Liu [a, c, 1], Dingding Gao [d, 1], Ting Wang [a], Tiantian Chen [a], Guirui Yan [a], Kaixian Chen [a], Yechun Xu [a, *], Heyao Wang [a, *], Yingxia Li [d, *], Weiliang Zhu [a, *]

[a] Drug Discovery and Design Center, Key Laboratory for Receptor Research, Shanghai Institute of Materia Medica, Chinese Academy of Sciences, 555 Zuchongzhi Road, Shanghai 201203, China
[b] Department of Pathophysiology, Key Laboratory of Cell Differentiation and Apoptosis of Chinese Ministry of Education, Shanghai JiaoTong University, School of Medicine, Shanghai, China
[c] School of Life Science and Technology, Shanghai Tech University, Shanghai 200031, China
[d] School of Pharmacy, Fudan University, 826 Zhangheng Road, Shanghai 201203, China

ARTICLE INFO

Article history:
Received 3 July 2014
Received in revised form
8 November 2014
Accepted 10 November 2014
Available online 11 November 2014

Keywords:
FABP4
Inhibitor
Diabetes
Virtual screening
Crystal structure

ABSTRACT

Fatty acid binding protein 4 (FABP4) is a potential drug target for diabetes and atherosclerosis. For discovering new chemical entities as FABP4 inhibitors, structure-based virtual screening (VS) was performed, bioassay demonstrated that 16 of 251 tested compounds are FABP4 inhibitors, among which compound **m1** are more active than endogenous ligand linoleic acid (LA). Based on the structure of **m1**, new derivatives were designed and prepared, leading to the discovery of two more potent inhibitors, compounds **9** and **10**. To further explore the binding mechanisms of these new inhibitors, we determined the X-ray structures of the complexes of FABP4-**9** and FABP4-**10**, which revealed similar binding conformations of the two compounds. Residue Ser53 and Arg126 formed direct hydrogen bonding with the ligands. We also found that **10** could significantly reduce the levels of lipolysis on mouse 3T3-L1 adipocytes. Taken together, *in silico*, *in vitro* and crystallographic data provide useful hints for future development of novel inhibitors against FABP4.

© 2014 Elsevier Masson SAS. All rights reserved.

1. Introduction

Fatty acids function both as energy source and as signals for metabolic regulation in mammalian cells. Chaperones of fatty acids are commonly known as fatty acid binding proteins (FABPs) that act as fatty acids shuttles and play important roles in metabolic and inflammatory diseases [1–3]. Since the initial discovery of FABPs in 1972, at least nine members have been identified.

FABP4, also known as A-FABP or aP2, was first detected in mature adipocytes and adipose tissues. It plays a significant role in many aspects of metabolic syndrome [4,5]. Disruption of FABP4 in mice prevents them from diet-induced insulin resistance [6,7], while macrophage-specific deletion of FABP4 leads to protection of atherosclerosis in apolipoprotein E-deficient mice [8]. Reduced FABP4 expression in adipose tissue in human being showed lower serum triglyceride levels and significantly reduced risk of type 2 diabetes [9]. Increasing evidences indicate that pharmacological agents that modify FABP4 function may offer therapeutic opportunities for metabolic syndrome. Indeed, several series of small-molecule inhibitors of FABP4 have been reported over the last decade [10–17]. For example, BMS309403, a highly active inhibitor of FABP4, demonstrated to be effective to improve glucose metabolism, enhance insulin sensitivity in both dietary and genetic mouse models of obesity and diabetes, and ameliorate the symptom of atherosclerosis [18]. The above studies indicated the potential application of FABP4 inhibitors in the treatment of diabetes and atherosclerosis.

To date, several crystal structures of human FABP4 have been determined for apo and holo forms (bound with various ligands) [13–16,19,20]. Structurally, FABP4 is composed of a well-known assembly of ten antiparallel β-strands and a helix-loop-helix cap in the N-terminal. The complex structures of FABP4 and various

* Corresponding authors.
E-mail addresses: ycxu@simm.ac.cn (Y. Xu), wlzhu@mail.shcnc.ac.cn (W. Zhu).
[1] These authors contributed equally to the work.

http://dx.doi.org/10.1016/j.ejmech.2014.11.020
0223-5234/© 2014 Elsevier Masson SAS. All rights reserved.

ligands provide insight into the structural foundation underlying the binding modes of endogenous ligands and small molecule inhibitors in the active pocket of FABP4.

These results inspire us to discover and design novel inhibitors of FABP4 via the current state-of-the-art structure-based approach. We reported a novel types of FABP4 inhibitors discovered by virtual screening [11]. Here, we report another type of small-molecule inhibitors. Starting from the structure of **m1** (Fig. 1), which was discovered via virtual screening, we designed and synthesized a series of new 2,4,6-triisopropylbenzene derivatives, leading to the discovery of more potent compounds **9** and **10**. X-ray crystallography was then applied to study the binding mechanisms between FABP4 and the new compounds.

2. Results and discussion

2.1. Virtual screening and biological evaluation

In an effort to discover novel inhibitors of FABP4, two chemical databases: Specs (http://www.specs.net) and Maybridge (http://www.maybridge.com) were virtually screened against the target protein FABP4. The X-ray structure of FABP4 binding with BMS309403 (PDB code: 2NNQ [14]) was retrieved from the Protein Data Bank (http://www.rcsb.org/pdb) for docking calculation. Specs compounds (~200,000 compounds) were first filtered with our in-house script Druglk, leading to 80,000 compounds left. Then similar procedure to our previous work was applied for the virtual screening of FABP4 inhibitors in this study [11]. Briefly, the databases Maybridge and Specs were filtered by software DOCK4.0 [21], the top 10% ranked compounds with the highest score were selected by software GLIDE [22,23] (www.schröinger.com). Then the top 800 and 300 compounds from Maybridge and Specs, respectively, were rescored by AUTODOCK3 program [24]. Taking into account both Glide and AUTODOCK3 scores, 52 and 199 molecules from Maybridge and Specs were finally selected and purchased from the vendors. The inhibitory activity of the purchased compounds were determined using the 1,8-ANS ligand displacement assay as described in our previous study [11]. Primary bioassay was performed at 100 μM, 11 compounds showed inhibitory activity against FABP4 (6 for Specs and 5 for Maybridge). Based on these hits, a structural similarity-based search in the two databases was performed. Another 36 compounds were purchased from Maybridge, leading to the discovery of another 5 hits. However, none were purchased from Specs because no highly similar structures were identified in the database. Thus, 16 FABP4 inhibitors in total were discovered through the two-step virtual screening and bioassay approach. One series of the active compounds (10 compounds) have been reported in our previous study [11]. The rest 6 active compounds are sulfonamides, among which compound **m1** demonstrated highest FABP4 inhibition with an IC_{50} value of 16.8 μM (Table 1, Fig. 1), which was slightly more active than the endogenous ligand linoleic acid (LA, 17.7 μM, Table 1).

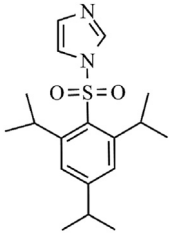

m1

Fig. 1. Structure of **m1**.

2.2. Compound design and synthesis

Starting from the molecular structure of **m1** and the docked complex structure of FABP4-**m1**, we designed and synthesized a new series of 2,4,6-triisopropylbenzene derivatives mainly focusing on the replacement of imidazole with benzimidazole and benzimidazole analogs (Schemes 1–3). In general, treatment of appropriate commercially available substituted diaminobenzene with triethyl orthoformate or triethyl orthoacetate and CH_3OH under the

Table 1
Inhibitory activities of newly designed and synthesized benzimidazole analogs.

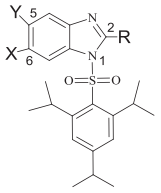

R=H,CH_3
X=H,CH_3,Br,Cl,OCH_3,NO_2
Y=H,CH_3,Br,Cl,OCH_3,NO_2,NH_2

Compound	R	X	Y	Inhibition at 100 μM[a] (%)	IC_{50} (mean ± SE (μM))
Linoleic acid (LA)	–	–	–	85.0	17.7 ± 0.20
m1	–	–	–	87.8	16.8 ± 0.18
1	H	H	H	<10.0	NT
2a	CH_3	H	H	36.3	>100.0
2c	H	H	CH_3	<10.0	NT
2d	CH_3	CH_3	H	<10.0	NT
2e	CH_3	H	CH_3	<10.0	NT
3a	CH_3	Br	H	53.6	82.8 ± 0.91
3b	H	Br	H	92.2	14.8 ± 0.29
3c	H	H	Br	<10.0	NT
3d	CH_3	H	Br	<10.0	NT
4a	CH_3	Cl	H	<10.0	NT
4b	H	Cl	H	<10.0	NT
4c	H	H	Cl	<10.0	NT
4d	CH_3	H	Cl	90.8	14.8 ± 0.26
5a	CH_3	OCH_3	H	<10.0	NT
5b	H	OCH_3	H	<10.0	NT
5c	H	H	OCH_3	<10.0	NT
5d	CH_3	H	OCH_3	<10.0	NT
6b	H	NO_2	H	<10.0	NT
6c	H	H	NO_2	<10.0	NT
7	H	NH_2	H	10.0	>100.0
8	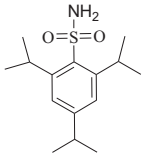			13.3	>100.0
9	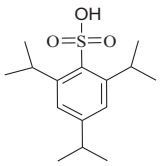			92.1	7.9 ± 0.086
10	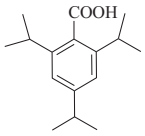			96.0	4.0 ± 0.043

NT: not determined.
[a] Values are means of triplicate experiments with relative standard deviations <10%, the data were analyzed with GraphPad Prism software.

promotion of $ZrCl_4$ afforded **11a**–**h**. Then **11a**–**h** reacted with 2,4,6-triisopropylbenzenesulfonyl chloride and triethylamine to give **2**–**5** (Scheme 1). Because benzimidazole ring has the phenomenon of tautomerism in the solution, compounds **11a**–**h** and 6-nitrobenzimidazole reacted with 2,4,6-triisopropylbenzenesulfonyl chloride to give both 5-substituted and 6-substituted products. The ratio of them was about 1:1.

The target compounds **1** and **2a** were synthesized by commercially available 2-substituted benzimidazole reacting with 2,4,6-triisopropylbenzenesulfonyl chloride in the presence of triethylamine as shown in Scheme 2. Compound **6b** and **6c** were prepared in a similar manner as described for compound **1** started from commercially available 6-nitrobenzimidazole. A suspension of **6b** and Pd/C in CH_2Cl_2–MeOH under H_2 at room temperature to give compound **7** as shown in Scheme 3.

The preparation of the target compounds **8**, **9** and **10** was performed as shown in Scheme 4. The target compound **8** was prepared from 2,4,6-triisopropylbenzene-sulfonyl chloride by reaction with $NH_3 \cdot H_2O$ in THF. Reflux of 2,4,6-triisopropylbenzenesulfonyl chloride in H_2O/dioxane (v/v,1:1) to provide compound **9**. Compound **10** was produced by the reaction of 2,4,6-triisopropylbenzoyl chloride with triethylamine in acetone in 99% yield.

2.3. In vitro FABP4 inhibition assay

The synthesized compounds were evaluated for their ability to inhibit FABP4. As shown in Table 1, 8 of the newly synthesized compounds showed inhibitory activities against FABP4 at 100 μM. Notably, compounds **9** and **10** were the most potent inhibitors against FABP4 with IC_{50} values of 7.9 and 4.0 μM, respectively. The bioassay result showed that the substitution of imidazole with benzimidazole (**1**) caused complete loss of inhibition (Table 1). Benzimidazole C^5-substituted compounds of **1** (**2c**, **3c**, **4c**, **5c**, **6c**) exhibited no activities against FABP4 at 100 μM, either. However, increased inhibitory activity was observed when a methyl group was introduced into the position C^2 of the benzimidazole group (**2a**, Table 1). Moreover, compound **4d**, with a methyl group at the position C^2 of the benzimidazole group of **4c**, showed pretty high potency against FABP4 with an IC_{50} value of 14.8 μM (Table 1).

FABP4 inhibitory activity of the analogs was significantly affected by the type of chemical modifications on the position C^6 (**3b**, **4b**, **5b**, **6b**, **7**). The bioassay results revealed that C^6-amino substituted **7** showed weak inhibitory activity, while **3b** with halogen substituent exhibited high potency (IC_{50} 14.8 μM).

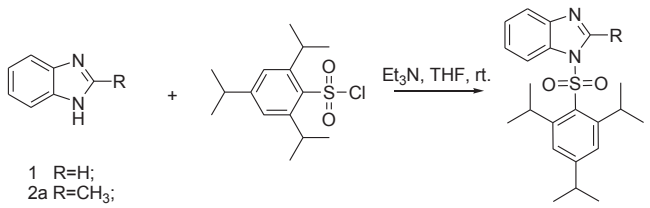

Scheme 2. Scheme for the synthesis of **1** and **2a**.

However, **3a** with a methyl group at the position C^2 of the benzimidazole group, showed reduced activity (IC_{50} 82.8 μM).

The most active inhibitors of **m1** analogs, namely **3b** and **4d**, had similar activity to **m1**. Thus, the replacement of imidazole with benzimidazole analogs has no significant effect on activity. Studies have revealed that small molecules with acid groups showed high inhibitory activity against FABP4 [13,14], we then replaced the benzimidazole group with a hydroxyl group (**9**). Indeed, the inhibitory activity of **9** increased remarkably with an IC_{50} value of 7.9 μM. When the sulfonic acid group was substituted by carboxylic acid group (**10**), the inhibitory activity increased nearly 2-fold again (Table 1).

FABP3-deficient mice showed reduced exercise tolerance, and developed regional cardiac hypertrophy at old age, indicating that FABP3 played an important role in metabolic homeostasis [25]. Therefore, the activity of **9** and **10** against FABP3 were also determined (Table 2). **9** displayed 11.5-fold preferences over FABP3, while **10** showed 18.3-fold preferences over FABP3.

Fabp4 and *Fabp5* double-knockout mice demonstrated strong protection from diet-induced obesity (DIO), insulin resistance and type 2 diabetes [26]. Dual inhibition by both FABP4 and FABP5 was reported to be potentially useful for the treatment of dyslipidemia and/or diabetes. Thus, we also determined the inhibitory activities of **9** and **10** on FABP5. **9** demonstrated modest activity on FABP5 with an IC_{50} value of 16 μM while **10** is weak with the IC_{50} value higher than 50 μM. Thus, further structural optimization of these compounds is still needed for the development of more effective candidates to treat type 2 diabetes without side effects.

2.4. Lipolysis inhibition in 3T3-L1 adipocytes

As targeted deletion or chemical inhibition of FABP4 decreased lipolysis in adipocytes [12,27], we accessed whether **9** and **10** could modulate the levels of lipolysis on adipocytes. We used mouse 3T3-L1 adipocytes in this work, as FABP4 sequences and tertiary

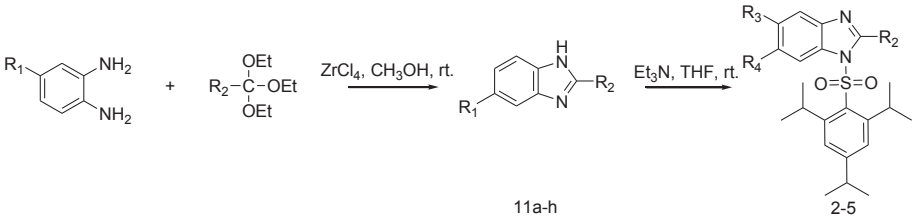

2c R_2=R_4=H, R_3=R_1=CH_3;
2d R_2=R_4=R_1=CH_3, R_3=H;
2e R_2=R_3=R_1=CH_3, R_4=H;
3a R_2=CH_3, R_3=H, R_4=R_1=Br;
3b R_2=R_3=H, R_4=R_1=Br;
3c R_2=R_4=H, R_3=R_1=Br;
3d R_2=CH_3, R_3=R_1=Br, R_4=H;
4a R_2=CH_3, R_3=H, R_4=R_1=Cl;
4b R_2=R_3=H, R_4=R_1=Cl;
4c R_2=R_4=H, R_3=R_1=Cl;
4d R_2=CH_3, R_3=R_1=Cl, R_4=H;
5a R_2=CH_3, R_3=H, R_4=R_1=OCH_3;
5b R_2=R_3=H, R_4=R_1=OCH_3;
5c R_2=R_4=H, R_3=R_1=OCH_3;
5d R_2=CH_3, R_3=R_1=OCH_3, R_4=H;

Scheme 1. Scheme for the synthesis of **2**–**5**.

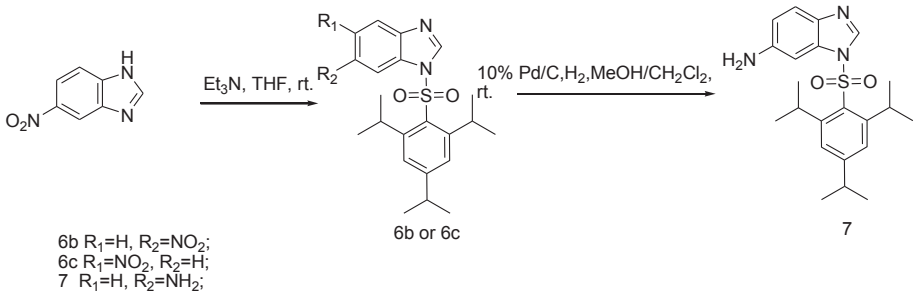

Scheme 3. Scheme for the synthesis of **6** and **7**.

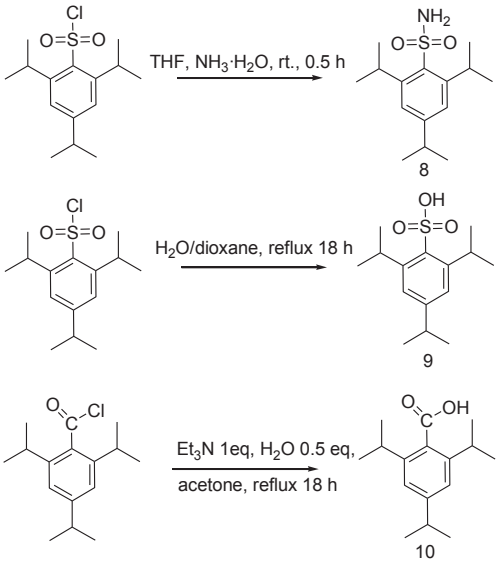

Scheme 4. Scheme for the synthesis of **8**–**10**.

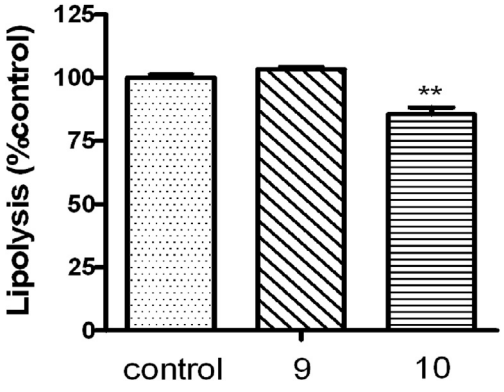

Fig. 2. Effect of **9** (50 μM) and **10** (50 μM) on forskolin-stimulated lipolysis in mouse 3T3-L1 adipocytes. Control: DMSO.

structures are highly conserved between human (PDB code: 2NNQ [14]) and mouse (PDB code: 3HK1 [12]). The result showed **10** could significantly reduce forskolin-stimulated lipolysis at dose level of 50 μM (Fig. 2). Although no effect was observed at 50 μM (Fig. 2), **9** reduced approximately 9.0% of the forskolin-stimulated lipolysis at 100 μM. These results are in agreement with our inhibitory activity data on FABP4 (Table 1). It confirmed that **9** and **10** are FABP4 inhibitors.

2.5. Binding mechanisms revealed by X-ray crystallography

To explore the binding mechanisms between FABP4 and the inhibitors, the complex structures of FABP4-**9** and FABP4-**10** were determined by X-ray crystallization. The FABP4 conformations that we obtained can align well with the previous reported structures. The complex structures revealed similar binding modes for the two compounds in the pocket of FABP4 (Fig. 3(A) and (B)). The 2,4,6-triisopropylbenzene groups lie in the hydrophobic region of the pocket defined by Met20, Val25, Ala33, Ala36, Phe57, Ala75 and Ile104 (Fig. 3(A) and (B)). In addition, the acid groups of both compounds (sulfonic acid group of **9** and carboxylic acid group of **10**) formed hydrogen bonds with the protein and four structural water molecules (Ser53, Thr60, Arg106, Arg126, Tyr128; Fig. 3).

Although the X-ray structures provided detailed binding information between FABP4 and the two compounds, the mechanisms for activity differences between the benzimidazole analogs were still unclear. To further explore the binding mechanism between other benzimidazole analogs with FABP4, **4d** was docked into the binding pocket of FABP4 by AUTODOCK4 [24]. The crystal results demonstrated that the acid groups of **9** and **10** formed main polar interactions with 3 key residues of FABP4 (Arg106, Arg126, Tyr128, Fig. 3). The docking result showed that sulfonyl group formed polar interactions with residue Arg126 and Tyr128 of FABP4, but not Arg106 (Fig. 4). This might be one of the reasons that **4d** and other benzimidazole analogs had weaker inhibitory activities than **9** or **10**. The docking result also revealed hydrophobic interactions between residue Met40, Ile115 and Arg128 and the methyl group at the position C^2 of the benzimidazole. This methyl group might help to stabilize the conformation of the ligand. Thus when a methyl group was introduced into the position C^2 of the benzimidazole group (**2a**, Table 1), it showed moderate activity, and those without methyl group at the position C^2 (**2c**, **3c**, **4c**, **5c**, **6c**) showed no activities except **3b**. Moreover, polar groups with small volume, such as Cl, might be favored at the position C^5 as shown in Fig. 4. The

Table 2
Selectivity of the tested FABP4 inhibitors over FABP3.

Compound	FABP4 IC_{50}[a] (μM)	FABP3 IC_{50}[b] (μM)	Selectivity index FABP3/FABP4
Linoleic acid (LA)	1.0	1.0	1.0
9	0.45	5.16	11.5
10	0.23	4.20	18.3

[a] Values are means of triplicate experiments with relative standard deviations <10%, presented as the fold of LA on FABP4.
[b] Values are means of triplicate experiments with relative standard deviations <10%, presented as the fold of LA on FABP3.

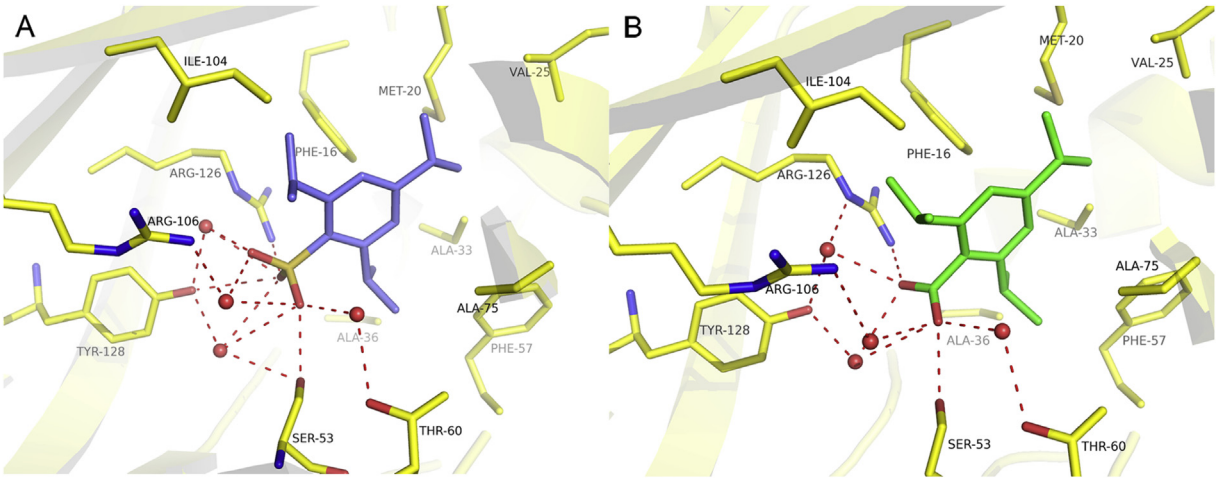

Fig. 3. X-ray crystal structures of **9** (A) and **10** (B) binding to the active site of FABP4. The dashed lines in red represent hydrogen bonds. Compounds **9** (slate) and **10** (green) are shown in sticks. Residues of FABP4 are shown in yellow sticks. Waters are shown as red balls. (For interpretation of the references to colour in this figure legend, the reader is referred to the web version of this article.)

above results should also be helpful for further structural optimization of FABP4 inhibitors.

3. Conclusion

In summary, we carried out virtual screening to identify novel inhibitors of FABP4. Based on the structure of the most active hit **m1**, structural modifications by the replacement of imidazole with benzimidazole and benzimidazole analogs were carried out. The bioassay demonstrated eight new compounds had inhibitory activities against FABP4. Among them, compounds **9** and **10** were the most potent compounds against FABP4, with IC_{50} 7.9 μM and 4.0 μM, respectively. Moreover, **10** could reduce forskolin-stimulated lipolysis at dose level of 50 μM. X-ray crystallography and further docking results demonstrated the binding mechanisms between the ligands and FABP4. Our results provide useful information for further development of FABP4 inhibitors.

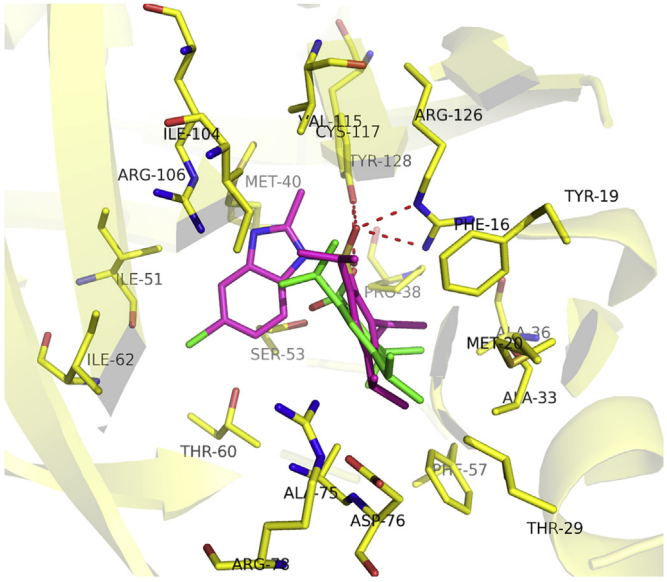

Fig. 4. Predicted binding conformation of **4d** (magenta) aligned with **10** (green) in the crystal structure of FABP4. The dashed lines in red represent hydrogen bonds. Compounds **4d** and **10** are shown in sticks. Residues of FABP4 are shown in yellow sticks. (For interpretation of the references to colour in this figure legend, the reader is referred to the web version of this article.)

4. Experimental

4.1. Chemistry

Melting points were measured on an SGW X-4 melting point apparatus without correction. The type of analytical thin-layer chromatography (TLC) was HSGF 254 (0.15–0.2 mm thickness, Yantai Jiangyou Company, China). ^{1}H NMR and ^{13}C NMR spectra were taken on a Varian/Mercury Plus 400 spectrometer with tetramethylsilane as an internal standard. Chemical shifts were reported in parts per million (ppm, δ) downfield from tetramethylsilane. Proton coupling patterns were described as singlet (s), doublet (d), triplet (t), quartet (q), multiplet (m), and broad (br). Mass spectra were given with electric (EI) produced by Agilent 1100LC/MSD mass spectrometer.

4.1.1. 1-(2,4,6-Triisopropylphenylsulfonyl)-1H-benzo[d]imidazole (**1**)

A solution of benzimidazole (550 mg, 4.66 mmol) in anhydrous THF (10 mL) and triethylamine (0.67 mL, 4.66 mmol) was stirred for 0.5 h, then treated with 2,4,6-triisopropylbenzenesulfonyl chloride (1.41 g, 4.66 mmol) in anhydrous THF (5 mL), and refluxed for 12 h until TLC indicated that the reaction was complete. The resulting precipitate of triethylammonium chloride was filtered off. The solution was concentrated under reduced pressure. The residue was purified by silica gel column chromatography (8:1, v/v, petroleum ether/EtOAc) to give **1** (1.467 g, 82%) as a white solid; $\mathbf{R_f} = 0.6$ (1:4, EtOAc:Petroleum ether); mp 142–144 °C; ^{1}H NMR (DMSO): δ 8.80 (s, 1H, C<u>H</u>–N), 7.75–7.72 (m, 1H, Ar–<u>H</u>), 7.33 (s, 2H, Ar–<u>H</u>), 7.31–7.26 (m, 2H, Ar–<u>H</u>), 7.10–7.07 (m, 1H, Ar–<u>H</u>), 4.06–3.99 (m, 2H, 2 × C<u>H</u>(CH$_3$)$_2$), 2.92–2.88 (m, 1H, C<u>H</u>(CH$_3$)$_2$), 1.14 (d, 6H, J = 6.7 Hz, 2 × C<u>H</u>$_3$), 1.01 (d, 12H, J = 6.7 Hz, 4 × C<u>H</u>$_3$); ^{13}C NMR (DMSO): δ 147.3, 146.8, 140.7, 130.6, 126.0, 121.4, 114.5, 33.3, 28.0, 24.8; ESI-MS m/z: 385.1 ([M+H]$^+$).

4.1.2. 2-Methyl-1-(2,4,6-triisopropylphenylsulfonyl)-1H-benzo[d]imidazole (**2a**)

Compound **2a** was prepared as a white solid in a similar manner as described for compound **1**. Yield: 35%; $\mathbf{R_f}$ = 0.6 (1:4,

EtOAc:Petroleum ether); mp 104–105 °C; ^{1}H NMR (DMSO): δ 7.62–7.59 (m, 1H, Ar–H), 7.56–7.54 (m, 1H, Ar–H), 7.32 (s, 2H, Ar–H), 7.30–7.28 (m, 2H, Ar–H), 3.90–3.83 (m, 2H, 2 × CH(CH$_3$)$_2$), 2.94–2.91 (m, 1H, CH(CH$_3$)$_2$), 2.28 (s, 3H, CH$_3$), 1.15 (d, 6H, J = 6.7 Hz, 2 × CH$_3$), 0.93 (d, 12H, J = 6.7 Hz, 4 × CH$_3$); ^{13}C NMR (CDCl$_3$): δ 155.5, 151.6, 151.1, 141.4, 134.2, 132.2, 124.7, 124.5, 119.8, 113.3, 34.5, 29.7, 24.4; ESI-MS m/z: 400.0 ([M+H]$^+$).

*4.1.3. General procedure for the preparation of 2,5-substituted-1H-benzo[d]imidazole or 2,6-substituted-1H-benzo[d]imidazole (**11a–h**)*

A mixture of o-phenylenediamine (1.0 mmol), triethyl orthoformate (1.2 mmol) and $ZrCl_4$ (0.1 mmol) in 10 mL MeOH was stirred at room temperature for 3 h. After completion of the reaction, as indicated by TLC, the solvent was concentrated and the resulting product was directly purified by silica gel column chromatography (4:1 → 1:1, v/v, petroleum ether/EtOAc) to afford compound **11a–h**.

*4.1.3.1. 6-Methyl-1H-benzo[d]imidazole (**11a**).* A white solid, yield 100%; $\mathbf{R_f}$ = 0.4 (1:20, CH_2Cl_2:CH_3OH); ^{1}H NMR (CDCl$_3$): δ 8.1 (s, 1H, CH–N), 7.58 (d, 1H, J = 8.3 Hz, Ar–H), 7.46 (s, 1H, Ar–H), 7.13 (dd, 1H, J = 1.2, 8.3 Hz, Ar–H), 2.49 (s, 3H, Ar–CH$_3$); ^{13}C NMR (CDCl$_3$): δ 140.5, 137.5, 136.4, 132.7, 124.3, 115.4, 114.8, 21.6.

*4.1.3.2. 2,6-Dimethyl-1H-benzo[d]imidazole (**11b**).* A white solid, yield 96%; $\mathbf{R_f}$ = 0.2 (1:1, EtOAc:Petroleum ether); ^{1}H NMR (CDCl$_3$): δ 7.45 (d, 1H, J = 8.3 Hz, Ar–H), 7.33 (s, 1H, Ar–H), 7.04 (d, 1H, J = 7.9 Hz, Ar–H), 2.62 (s, 3H, CH$_3$), 2.46 (s, 3H, CH$_3$); ^{13}C NMR (CDCl$_3$): δ 150.9, 138.5, 137.1, 131.9, 123.5, 114.3, 114.0, 21.6, 14.9.

*4.1.3.3. 5-Bromo-1H-benzo[d]imidazole (**11c**).* A brown solid, yield 95%; $\mathbf{R_f}$ = 0.1 (1:1, EtOAc:Petroleum ether); ^{1}H NMR (CDCl$_3$): δ 8.10 (s, 1H, CH–N), 7.87 (s, 1H, Ar–H), 7.52 (d, 1H, J = 8.6 Hz, Ar–H), 7.46 (d, 1H, J = 8.2 Hz, Ar–H).

*4.1.3.4. 5-Bromo-2-methyl-1H-benzo[d]imidazole (**11d**).* A light gray solid, yield 87%; $\mathbf{R_f}$ = 0.1 (1:1, EtOAc:Petroleum ether); ^{1}H NMR (CDCl$_3$): δ 7.67 (s, 1H, Ar–H), 7.39 (d, 1H, J = 8.6 Hz, Ar–H), 7.32 (d, 1H, J = 8.2 Hz, Ar–H), 2.62 (s, 3H, CH$_3$).

*4.1.3.5. 5(6)-Chloro-1H-benzo[d]imidazole (**11e**).* A white solid, yield 100%; $\mathbf{R_f}$ = 0.3 (20:1, CH_2Cl_2:CH_3OH); ^{1}H NMR (CDCl$_3$): δ 8.36 (d, 1H, J = 9.8 Hz, Ar–H), 8.11 (s, 2H, CH), 7.71 (d, 1H, J = 8.6 Hz, Ar–H), 7.66 (d, 2H, J = 2.0 Hz, Ar–H), 7.58 (d, 2H, J = 8.6 Hz, Ar–H), 4.98 (br s, 2H, 2 × NH); ^{13}C NMR (CDCl$_3$): δ 142.3, 141.7, 138.1, 136.5, 135.7, 128.7, 126.4, 125.8, 116.4, 115.4, 29.6, 23.6.

*4.1.3.6. 5-Chloro-2-methyl-1H-benzo[d]imidazole (**11f**).* A white solid, yield 100%; $\mathbf{R_f}$ = 0.3 (20:1, CH_2Cl_2:CH_3OH); ^{1}H NMR (CDCl$_3$): δ 7.53 (d, 1H, J = 2.0 Hz, Ar–H), 7.44 (d, 1H, J = 8.6 Hz, Ar–H), 7.20 (dd, 1H, J = 2.0, 8.2 Hz, Ar–H), 2.64 (s, 3H, CCH$_3$); ^{13}C NMR (CDCl$_3$): δ 152.0, 128.0, 122.9, 115.2, 114.5, 109.7, 15.0.

*4.1.3.7. 6-Methoxy-1H-benzo[d]imidazole (**11g**).* A black solid, yield 68%; $\mathbf{R_f}$ = 0.1 (1:1, EtOAc:Petroleum ether); ^{1}H NMR (CDCl$_3$): δ 8.03 (s, 1H, CH–N), 7.56 (d, 1H, J = 8.7 Hz, Ar–H), 7.11 (d, 1H, J = 1.6 Hz, Ar–H), 6.94 (dd, 1H, J = 2.0, 8.7 Hz, Ar–H), 3.84 (s, 3H, OCH$_3$).

*4.1.3.8. 6-Methoxy-2-methyl-1H-benzo[d]imidazole (**11h**).* A black solid, yield 92%; $\mathbf{R_f}$ = 0.1 (1:1, EtOAc:Petroleum ether); ^{1}H NMR (CDCl$_3$): δ 7.42 (d, 1H, J = 8.7 Hz, Ar–H), 7.02 (d, 1H, J = 2.0 Hz, Ar–H), 6.86 (dd, 1H, J = 2.4, 8.7 Hz, Ar–H), 3.83 (s, 3H, OCH$_3$), 2.60 (s, 3H, CH$_3$).

*4.1.4. General procedure for the preparation of 2,5-trimethyl-1-(2,4,6-triisopropylphenylsulfonyl)-1H-benzo[d]imidazole or 2,6-trimethyl-1-(2,4,6-triisopropylphenylsulfonyl)-1H-benzo[d] imidazole (**2c–5d**)*

Compounds **2c–5d** were prepared in a similar manner as described for compound **1** started from appropriate substituted benzimidazole **11a–h**.

*4.1.4.1. 5-Methyl-1-(2,4,6-triisopropylphenylsulfonyl)-1H-benzo[d] imidazole (**2c**).* A white solid, yield 85%; $\mathbf{R_f}$ = 0.6 (1:4, EtOAc:Petroleum ether); mp 154–155 °C; ^{1}H NMR (CDCl$_3$): δ 8.28 (s, 0.3H, CH–N), 8.26 (s, 1H, CH–N), 7.64 (d, 1H, J = 8.2 Hz, Ar–H), 7.56 (s, 0.3H, Ar–H), 7.22 (s, 2H, Ar–H), 7.21 (s, 0.7H, Ar–H), 7.15 (d, 1H, J = 5.9 Hz, Ar–H), 7.11 (d, 1H, J = 6.7 Hz, Ar–H), 4.24–4.15 (m, 2H, 2 × CH(CH$_3$)$_2$), 2.94–2.91 (m, 1H, CH(CH$_3$)$_2$), 2.46 (s, 1H, CH$_3$), 2.38 (s, 3H, CH$_3$), 1.25 (d, 6H, J = 7.0 Hz, 2 × CH$_3$), 1.14 (d, 12H, J = 6.7 Hz, 4 × CH$_3$); ^{13}C NMR (CDCl$_3$): δ 155.5, 155.5, 151.7, 151.6, 141.5, 140.5, 140.0, 135.3, 131.4, 126.6, 125.8, 124.5, 120.8, 120,4, 111.7, 34.3, 29.6, 24.4, 23.4; ESI-MS m/z: 400.0 ([M+H]$^+$).

*4.1.4.2. 2,6-Trimethyl-1-(2,4,6-triisopropylphenylsulfonyl)-1H-benzo[d]imidazole (2d); 2,5-trimethyl-1-(2,4,6-triisopropyl-phenylsulfonyl)-1H-benzo[d]imidazole (**2e**).* **A** white solid of mixture of **2d** and **2e**, yield 85%; $\mathbf{R_f}$ = 0.6 (1:4, EtOAc:Petroleum ether); mp 125–127 °C (mixture of **2d** and **2e**); ^{1}H NMR (CDCl$_3$): δ 7.65 (dd, 1H, J = 0.8, 7.8 Hz, Ar–H), 7.52 (d, 2H, J = 6.3 Hz, Ar–H), 7.43 (s, 1H, Ar–H), 7.27 (d, 2H, J = 2.4 Hz, Ar–H), 7.18 (s, 2H, Ar–H), 7.11 (d, 2H, J = 7.8 Hz, Ar–H), 4.07–4.03 (m, 4H, 4 × CH(CH$_3$)$_2$), 2.94–2.90 (m, 2H, 2 × CH(CH$_3$)$_2$), 2.45 (s, 6H, 2 × CH$_3$), 2.43 (s, 3H, CH$_3$), 2.39 (s, 3H, CH$_3$), 1.25 (d, 12H, J = 7.0 Hz, 4 × CH$_3$), 1.04 (d, 24H, J = 6.7 Hz, 8 × CH$_3$); ^{13}C NMR (CDCl$_3$): δ 155.2155.1, 151.3, 150.7, 141.4, 139.2, 134.4, 134.0, 133.6, 132.0, 131.9, 125.7, 125.2, 124.2, 119.5, 119.0, 113.0, 112.5, 34.2, 29.4, 24.1, 21.8, 21.3, 20.7, 16.0, 15.9; ESI-MS m/z: 414.0 ([M+H]$^+$).

*4.1.4.3. 6-Bromo-2-methyl-1-(2,4,6-triisopropylphenylsulfonyl)-1H-benzo[d]imidazole (**3a**).* A white solid, yield 17%; $\mathbf{R_f}$ = 0.7 (1:4, EtOAc:Petroleum ether); mp 106–107 °C; ^{1}H NMR (CDCl$_3$): δ 7.80 (d, 1H, J = 1.8 Hz, Ar–H), 7.69 (d, 1H, J = 8.9 Hz, Ar–H), 7.42 (dd, 1H, J = 2.0, 8.9 Hz, Ar–H), 7.20 (s, 2H, Ar–H), 4.02–3.96 (m, 2H, 2 × CH(CH$_3$)$_2$), 2.96–2.90 (m, 1H, CH(CH$_3$)$_2$), 2.38 (s, 3H, =CCH$_3$), 1.26 (d, 6H, J = 6.7 Hz, 2 × CH$_3$), 1.04 (d, 12H, J = 6.7 Hz, 4 × CH$_3$); ^{13}C NMR (CDCl$_3$): δ 155.6, 151.4, 142.5, 133.0, 131.6, 127.4, 124.3, 122.6, 117.0, 114.3, 34.3, 29.5, 24.1, 15.8; ESI-MS m/z: 477.9 ([M+H]$^+$).

*4.1.4.4. 6-Bromo-1-(2,4,6-triisopropylphenylsulfonyl)-1H-benzo[d] imidazole (**3b**).* A white solid, yield 13%; $\mathbf{R_f}$ = 0.5 (1:4, EtOAc:Petroleum ether); mp 168–169 °C; ^{1}H NMR (CDCl$_3$): δ 8.32 (s, 1H, CH–N), 7.64 (d, 1H, J = 8.6 Hz, Ar–H), 7.44 (s, 1H, Ar–H), 7.42 (dd, 1H, J = 2.0, 8.2 Hz, Ar–H), 7.24 (s, 2H, Ar–H), 4.19–4.12 (m, 2H, 2 × CH(CH$_3$)$_2$), 2.95–2.91 (m, 1H, CH(CH$_3$)$_2$), 1.26 (d, 6H, J = 7.1 Hz, 2 × CH$_3$), 1.15 (d, 12H, J = 6.7 Hz, 4 × CH$_3$); ^{13}C NMR (CDCl$_3$): δ 156.1, 151.9, 141.0, 129.5, 127.7, 124.7122.2, 118.6, 115.0, 34.3, 29.6, 24.4; ESI-MS m/z: 463.9 ([M+H]$^+$).

*4.1.4.5. 5-Bromo-1-(2,4,6-triisopropylphenylsulfonyl)-1H-benzo[d] imidazole (**3c**).* A white solid, yield 20%; $\mathbf{R_f}$ = 0.6 (1:4, EtOAc:Petroleum ether); mp 166–167 °C; ^{1}H NMR (CDCl$_3$): δ 8.29 (s, 1H, CH–N), 7.94 (d, 1H, J = 1.6 Hz, Ar–H), 7.39 (dd, 1H, J = 1.6, 8.3 Hz, Ar–H), 7.22 (s, 2H, Ar–H), 7.18 (d, 1H, J = 8.7 Hz, Ar–H), 4.13–4.09 (m, 2H, 2 × CH(CH$_3$)$_2$), 2.94–2.90 (m, 1H, CH(CH$_3$)$_2$), 1.25 (d, 6H, J = 7.1 Hz, 2 × CH$_3$), 1.12 (d, 12H, J = 6.7 Hz, 4 × CH$_3$); ^{13}C NMR (CDCl$_3$): δ 155.9, 151.7, 144.7, 141.6, 130.2, 128.3, 124.6, 117.5, 112.9, 34.3, 29.7, 24.4; ESI-MS m/z: 463.9 ([M+H]$^+$).

*4.1.4.6. 5-Bromo-2-methyl-1-(2,4,6-triisopropylphenylsulfonyl)-1H-benzo[d]imidazole (**3d**).* A white solid, yield 13%; $\mathbf{R_f}$ = 0.6 (1:4, EtOAc:Petroleum ether); mp 130–132 °C; ^{1}H NMR ($CDCl_3$): δ 7.88 (d, 1H, *J* = 1.6 Hz, Ar–H), 7.51 (d, 1H, *J* = 8.6 Hz, Ar–H), 7.42 (dd, 1H, *J* = 1.6, 8.6 Hz, Ar–H), 7.21 (s, 2H, Ar–H), 4.03–3.97 (m, 2H, 2 × CH(CH_3)$_2$), 2.95–2.92 (m, 1H, CH(CH_3)$_2$), 2.41 (s, 3H, =CCH_3), 1.23 (d, 6H, *J* = 7.1 Hz, 2 × CH_3), 1.06 (d, 12H, *J* = 6.7 Hz, 4 × CH_3); ^{13}C NMR ($CDCl_3$): δ 155.7, 151.4, 140.2, 134.6, 131.4, 127.3, 124.4, 120.7, 117.7, 116.1, 34.3, 29.5, 24.2, 23.4, 16.0; ESI-MS *m*/*z*: 477.9 ($[M+H]^+$).

*4.1.4.7. 6-Chloro-2-methyl-1-(2,4,6-triisopropylphenylsulfonyl)-1H-benzo[d]imidazole (**4a**).* A light yellow solid, yield 12%; $\mathbf{R_f}$ = 0.6 (1:4, EtOAc:Petroleum ether); mp 140–141 °C; ^{1}H NMR ($CDCl_3$): δ 7.74 (d, 1H, *J* = 9.0 Hz, Ar–H), 7.64 (d, 1H, *J* = 2.0 Hz, Ar–H), 7.28 (dd, 1H, *J* = 2.0, 9.0 Hz, Ar–H), 7.20 (s, 2H, Ar–H), 4.03–3.96 (m, 2H, 2 × CH(CH_3)$_2$), 2.95–2.91 (m, 1H, CH(CH_3)$_2$), 2.38 (s, 3H, =CCH_3), 1.26 (d, 6H, *J* = 7.0 Hz, 2 × CH_3), 1.04 (d, 12H, *J* = 6.7 Hz, 4 × CH_3); ^{13}C NMR ($CDCl_3$): δ152.3, 151.4, 142.1, 132.6, 131.6, 129.6, 124.7, 124.3, 119.5, 113.4, 112.3, 34.3, 29.7, 24.2, 15.9; ESI-MS *m*/*z*: 433.9 ($[M+H]^+$).

*4.1.4.8. 6-Chloro-1-(2,4,6-triisopropylphenylsulfonyl)-1H-benzo[d]imidazole (**4b**).* A light yellow solid, yield 27%; $\mathbf{R_f}$ = 0.6 (1:4, EtOAc:Petroleum ether); mp 155–157 °C; ^{1}H NMR ($CDCl_3$): δ 8.31 (s, 1H, CH–N), 7.77 (d, 1H, *J* = 0.8 Hz, Ar–H), 7.25 (d, 1H, *J* = 1.6 Hz, Ar–H), 7.24 (s, 1H, Ar–H), 7.22 (s, 2H, Ar–H), 4.14–4.08 (m, 2H, 2 × CH(CH_3)$_2$), 2.94–2.90 (m, 1H, CH(CH_3)$_2$), 1.25 (d, 6H, *J* = 7.0 Hz, 2 × CH_3), 1.12 (d, 12H, *J* = 6.7 Hz, 4 × CH_3); ^{13}C NMR ($CDCl_3$, 100 MHz): δ 155.9, 151.7, 144.3, 141.8, 130.1, 129.8, 125.7, 124.6, 120.9, 112.5, 34.3, 29.7, 24.4; ESI-MS *m*/*z*: 420.0 ($[M+H]^+$).

*4.1.4.9. 5-Chloro-1-(2,4,6-triisopropylphenylsulfonyl)-1H-benzo[d]imidazole (**4c**).* A light yellow solid, yield 29%; $\mathbf{R_f}$ = 0.5 (1:4, EtOAc:Petroleum ether); mp 150–151 °C; ^{1}H NMR ($CDCl_3$): δ 8.31 (s, 1H, =CH–N), 7.69 (d, 1H, *J* = 9.0 Hz, Ar–H), 7.31–7.29 (m, 2H, Ar–H), 7.24 (s, 2H, Ar–H), 4.18–4.12 (m, 2H, 2 × CH(CH_3)$_2$), 2.95–2.92 (m, 1H, CH(CH_3)$_2$), 1.26 (d, 6H, *J* = 6.7 Hz, 2 × CH_3), 1.15 (d, 12H, *J* = 6.7 Hz, 4 × CH_3); ^{13}C NMR ($CDCl_3$): δ 156.0, 151.9, 142.1, 141.1, 131.1, 129.6, 125.1, 124.7, 121.8, 112.1, 34.3, 29.6, 24.4; ESI-MS *m*/*z*: 420.0 ($[M+H]^+$).

*4.1.4.10. 5-Chloro-2-methyl-1-(2,4,6-triisopropylphenylsulfonyl)-1H-benzo[d]imidazole (**4d**).* A light yellow solid, yield 15%; $\mathbf{R_f}$ = 0.5 (1:4, EtOAc:Petroleum ether); mp 111–112 °C; ^{1}H NMR ($CDCl_3$): δ 7.76 (d, 1H, *J* = 2.0 Hz, Ar–H), 7.56 (d, 1H, *J* = 8.6 Hz, Ar–H), 7.29 (dd, 1H, *J* = 2.0, 8.2 Hz, Ar–H), 7.21 (s, 2H, Ar–H), 4.04–3.97 (m, 2H, 2 × CH(CH_3)$_2$), 2.95–2.92 (m, 1H, CH(CH_3)$_2$), 2.40 (s, 3H, =CCH_3), 1.26 (d, 6H, *J* = 7.1 Hz, 2 × CH_3), 1.06 (d, 12H, *J* = 7.1 Hz, 4 × CH_3); ^{13}C NMR ($CDCl_3$): δ 155.7, 151.6, 151.4, 124.6, 124.4, 120.3, 113.3, 34.3, 29.5, 24.2, 16.0; ESI-MS *m*/*z*: 433.9 ($[M+H]^+$).

*4.1.4.11. 6-Methoxy-2-methyl-1-(2,4,6-triisopropylphenyl-sulfonyl)-1H-benzo[d]imidazole (**5a**).* A gray solid, yield 26%; $\mathbf{R_f}$ = 0.3 (1:5, EtOAc:Petroleum ether); mp 109–110 °C; ^{1}H NMR ($CDCl_3$): δ 7.65 (d, 1H, *J* = 9.1 Hz, Ar–H), 7.19 (s, 2H, Ar–H), 7.13 (d, 1H, *J* = 2.8 Hz, Ar–H), 6.91 (dd, 1H, *J* = 2.8, 9.1 Hz, Ar–H), 4.05–4.01 (m, 2H, 2 × CH(CH_3)$_2$), 3.85 (s, 3H, OCH_3), 2.93–2.89 (m, 1H, CH(CH_3)$_2$), 2.38 (s, 3H, =CCH_3), 1.27 (d, 6H, *J* = 7.1 Hz, 2 × CH_3), 1.04 (d, 12H, *J* = 6.7 Hz, 4 × CH_3); ^{13}C NMR ($CDCl_3$): δ 156.9, 155.2, 151.3, 142.2, 128.3, 124.2, 113.5, 113.3, 102.3, 55.6, 34.2, 29.7, 24.2, 15.9; ESI-MS *m*/*z*: 430.0 ($[M+H]^+$).

*4.1.4.12. 6-Methoxy-1-(2,4,6-triisopropylphenylsulfonyl)-1H-benzo[d]imidazole (**5b**).* A gray solid, yield 40%; $\mathbf{R_f}$ = 0.4 (1:5, EtOAc:Petroleum ether); mp 152–153 °C; ^{1}H NMR ($CDCl_3$): δ 8.23 (s, 1H, CH–N), 7.63 (d, 1H, *J* = 8.6 Hz, Ar–H), 7.22 (s, 2H, Ar–H), 6.91 (dd, 1H, *J* = 2.3, 8.6 Hz, Ar–H), 6.67 (d, 1H, *J* = 2.3 Hz, Ar–H), 4.16–4.12 (m, 2H, 2 × CH(CH_3)$_2$), 3.68 (s, 3H, OCH_3), 2.94–2.90 (m, 1H, CH(CH_3)$_2$), 1.25 (d, 6H, *J* = 6.7 Hz, 2 × CH_3), 1.12 (d, 12H, *J* = 6.7 Hz, 4 × CH_3); ^{13}C NMR ($CDCl_3$): δ 157.9, 155.6, 151.7, 139.3, 137.6, 132.0, 130.2, 124.5, 121.4, 113.7, 95.0, 55.6, 34.3, 29.7, 24.4; ESI-MS *m*/*z*: 415.9 ($[M+H]^+$).

*4.1.4.13. 5-Methoxy-1-(2,4,6-triisopropylphenylsulfonyl)-1H-benzo[d]imidazole (**5c**).* A gray solid, yield 38%; $\mathbf{R_f}$ = 0.3 (1:5, EtOAc:Petroleum ether); mp 134–135 °C; ^{1}H NMR ($CDCl_3$): δ 8.27 (s, 1H, =CH–N), 7.24 (d, 1H, *J* = 2.3 Hz, Ar–H), 7.21 (s, 2H, Ar–H), 7.16 (d, 1H, *J* = 9.0 Hz, Ar–H), 6.89 (dd, 1H, *J* = 2.3, 9.0 Hz, Ar–H), 4.17–4.13 (m, 2H, 2 × CH(CH_3)$_2$), 3.83 (s, 3H, OCH_3), 2.94–2.90 (m, 1H, CH(CH_3)$_2$), 1.25 (d, 6H, *J* = 7.0 Hz, 2 × CH_3), 1.13 (d, 12H, *J* = 7.0 Hz, 4 × CH_3); ^{13}C NMR ($CDCl_3$): δ 157.3, 155.5, 151.7, 144.5, 141.0, 130.2, 125.6, 124.5, 114.8, 112.0, 103.2, 55.7, 34.3, 29.6, 24.4; ESI-MS *m*/*z*: 415.9 ($[M+H]^+$).

*4.1.4.14. 5-Methoxy-2-methyl-1-(2,4,6-triisopropylphenyl-sulfonyl)-1H-benzo[d]imidazole (**5d**).* A gray solid, yield 25%; $\mathbf{R_f}$ = 0.4 (1:5, EtOAc:Petroleum ether); mp 103–104 °C; ^{1}H NMR ($CDCl_3$): δ 7.51 (d, 1H, *J* = 8.7 Hz, Ar–H), 7.19 (s, 2H, Ar–H), 7.18 (d, 1H, *J* = 2.4 Hz, Ar–H), 6.91 (dd, 1H, *J* = 2.4, 8.7 Hz, Ar–H), 4.05–4.01 (m, 2H, 2 × CH(CH_3)$_2$), 3.78 (s, 3H, OCH_3), 2.95–2.91 (m, 1H, CH(CH_3)$_2$), 2.42 (s, 3H,=CCH_3), 1.27 (d, 6H, *J* = 6.7 Hz, 2 × CH_3), 1.05 (d, 12H, *J* = 6.7 Hz, 4 × CH_3); ^{13}C NMR ($CDCl_3$): δ 157.4, 155.2, 151.3, 149.6, 135.4, 134.5, 124.2, 119.9, 112.8, 97.0, 55.8, 34.2, 29.5, 24.2, 16.1; ESI-MS *m*/*z*: 430.0 ($[M+H]^+$).

*4.1.5. 6-Nitro-1-(2,4,6-triisopropylphenylsulfonyl)-1H-benzo[d]imidazole (**6b**)*

Compound **6b** was prepared as a yellow solid in a similar manner as described for compound **1** started from commercially available 6-nitrobenzimidazole. Yield 46%; $\mathbf{R_f}$ = 0.6 (1:4, EtOAc:-Petroleum ether); mp 178–179 °C; ^{1}H NMR ($CDCl_3$): δ 8.60 (s, 1H, CH–N), 8.25 (dd, 1H, *J* = 2.1, 8.9 Hz, Ar–H), 8.13 (d, 1H, *J* = 1.8 Hz, Ar–H), 7.89 (d, 1H, *J* = 8.9 Hz, Ar–H), 7.27 (s, 2H, Ar–H), 4.20–4.13 (m, 2H, 2 × CH(CH_3)$_2$), 2.97–2.90 (m, 1H, CH(CH_3)$_2$), 1.25 (d, 6H, *J* = 7.0 Hz, 2 × CH_3), 1.17 (d, 12H, *J* = 6.7 Hz, 4 × CH_3); ^{13}C NMR ($CDCl_3$): δ 156.7, 152.0, 147.7, 145.2, 144.7, 130.6, 129.0, 125.0, 121.3, 120.0, 108.4, 34.3, 29.8, 24.4; ESI-MS *m*/*z*: 430.9 ($[M+H]^+$).

*4.1.6. 5-Nitro-1-(2,4,6-triisopropylphenylsulfonyl)-1H-benzo[d]imidazole (**6c**)*

Compound **6c** was prepared as a yellow solid in a similar manner as described for compound **1** started from commercially available 6-Nitrobenzimidazole. Yield 42%; $\mathbf{R_f}$ = 0.7 (1:4, EtOAc:-Petroleum ether); mp 158–160 °C; ^{1}H NMR ($CDCl_3$): δ 8.70 (s, 1H, CH–N), 8.44 (s, 1H, Ar–H), 8.23 (d, 1H, *J* = 8.9 Hz, Ar–H), 7.45 (d, 1H, *J* = 9.2 Hz, Ar–H), 7.25 (s, 2H, Ar–H), 4.12–4.05 (m, 2H, 2 × CH(CH_3)$_2$), 2.97–2.91 (m, 1H, CH(CH_3)$_2$), 1.25 (d, 6H, *J* = 7.0 Hz, 2 × CH_3), 1.13 (d, 12H, *J* = 6.7 Hz,4 × CH_3); ^{13}C NMR ($CDCl_3$): δ 156.5, 151.9, 145.0, 143.6, 143.2, 135.2, 129.4, 124.8, 120.7, 117.5, 112.0, 34.3, 29.8, 24.4; ESI-MS *m*/*z*: 430.9 ($[M+H]^+$).

*4.1.7. 1-(2,4,6-Triisopropylphenylsulfonyl)-1H-benzo[d]imidazole-6-amine (**7**)*

A suspension of **6b** (97 mg, 0.23 mmol) and Pd/C (80 mg, 10%) in CH_2Cl_2–MeOH (9:1, 20 mL) was stirred under H_2 for 2 h at room temperature and then filtered and concentrated. The residue was purified by silica gel column chromatography (5:1, v/v, petroleum ether/EtOAc) to give compound **7** (64.3 mg, 71%) as a yellow solid with $\mathbf{R_f}$ 0.4 (1:4, EtOAc:Petroleum ether); mp 152–153 °C; ^{1}H NMR ($CDCl_3$): δ 8.06 (s, 1H, CH–N), 7.53 (d, 1H, *J* = 8.6 Hz, Ar–H), 7.26 (s,

2H, Ar–H), 6.69 (s, 1H, Ar–H), 6.66 (s, 1H, Ar–H), 4.18–4.14 (m, 2H, 2 × CH(CH$_3$)$_2$), 3.72 (s, 2H, NH$_2$), 2.94–2.90 (m, 1H, CH(CH$_3$)$_2$), 1.26 (d, 6H, J = 6.7 Hz, 2 × CH$_3$), 1.14 (d, 12H, J = 6.7 Hz, 4 × CH$_3$); ^{13}C NMR (CDCl$_3$): δ 155.4, 151.6, 144.6, 138.5, 136.6, 132.5, 126.0, 124.5, 121.4, 113.5, 97.1, 34.2, 29.5, 24.5; ESI-MS m/z: 400.9 ([M+H]$^+$).

4.1.8. 2,4,6-Triisopropylbenzenesulfonamide (**8**)

To a solution of 2,4,6-triisopropylbenzenesulfonyl chloride (50 mg, 0.165 mmol) in THF (2 mL), NH$_3$·H$_2$O (0.127 mL, 25%) was added under stirring. The mixture was stirred for 0.5 h at room temperature until TLC indicated that the reaction was complete. The solvent was concentrated under reduced pressure. The residue was purified by silica gel column chromatography (1:5, v/v, EtOAc:Petroleum ether) to give **8** (48.3 mg, 98%) as a white solid; **R$_f$** = 0.3 (1:4, EtOAc:Petroleum ether); mp 121–122 °C(lit. [1] 119–119.6 °C); ^{1}H NMR (CDCl$_3$): δ 7.16 (s, 2H, Ar–H), 4.83 (s, 2H, NH$_2$), 4.14–4.07 (m, 2H, 2 × CH(CH$_3$)$_2$), 2.94–2.87 (m, 1H, CH(CH$_3$)$_2$), 1.29–1.24 (m, 18H, 6 × CH$_3$); ^{13}C NMR (CDCl$_3$): δ 152.8, 149.1, 123.7, 34.2, 29.8, 24.7; ESI-MS m/z: 282.3 ([M–H]$^-$).

4.1.9. 2,4,6-Triisopropylbenzenesulfonic acid (**9**)

2,4,6-Triisopropylbenzenesulfonyl chloride (50 mg, 0.165 mmol) was dissolved in a mixture of dioxane (5 mL) and water (10 mL) and heated under reflux for 24 h. The solvent was concentrated under reduced pressure. The residue was purified by silica gel column chromatography (20:1, v/v, CH$_2$Cl$_2$:MeOH) to give **9** (41.6 mg, 89%) as a white solid; **R$_f$** = 0.2 (20:1, CH$_2$Cl$_2$:CH$_3$OH); mp 260–262 °C; ^{1}H NMR (DMSO): δ 6.93 (s, 2H, Ar–H), 4.59–4.54 (m, 2H, 2 × CH(CH$_3$)$_2$), 2.80–2.76 (m, 1H, CH(CH$_3$)$_2$), 1.22 (d, 6H, J = 7.0 Hz, 2 × CH$_3$), 1.09 (d, 12H, J = 6.7 Hz, 4 × CH$_3$); ^{13}C NMR (DMSO): δ 147.2, 146.8, 141.8, 121.4, 33.3, 28.0, 24.8; ESI-MS m/z: 283.1 ([M-H]$^-$).

4.1.10. 2,4,6-Triisopropylbenzoic acid (**10**)

To a solution of 2,4,6-triisopropylbenzoyl chloride (100 mg, 0.375 mmol) in acetone (20 mL), Et$_3$N (54.2 μL, 0.375 mmol) and water (3.4 μL, 0.188 mmol) were added under stirring. The mixture was refluxed for 18 h until TLC indicated that the reaction was complete. The solvent was concentrated under reduced pressure. The residue was purified by silica gel column chromatography (1:10 → 1:5, v/v, EtOAc:Petroleum ether) to give **10** (92 mg, 99%) as a white solid; **R$_f$** = 0.8 (1:5, EtOAc:Petroleum ether); mp 186–187 °C; ^{1}H NMR (DMSO): δ 7.04 (s, 2H, Ar–H), 3.07–3.03 (m, 2H, 2 × CH(CH$_3$)$_2$), 2.92–2.89 (m, 1H, CH(CH$_3$)$_2$), 1.30–1.25 (m, 18H, 6 × CH$_3$); ^{13}C NMR (DMSO): δ 171.4, 149.0, 143.3, 132.0, 120.4, 33.6, 30.8, 23.8; ESI-MS m/z: 247.3 ([M–H]$^-$).

4.2. Virtual screening

Virtual screening was employed to search for novel FABP4 inhibitors. Two chemical databases: Specs (http://www.specs.net) and Maybridge (http://www.maybridge.com) were virtually screened against the target protein FABP4. The X-ray structure of FABP4 binding with BMS309403 (PDB code: 2NNQ [14]) was retrieved from the Protein Data Bank (http://www.rcsb.org/pdb) for docking calculation. For the screening of database Maybridge, the procedure has been reported in our previous study [11]. 52 compounds were finally purchased from the vendor.

For Specs, similar methods were used. First, we filtered the ~200,000 compounds with our in-house script Druglk, leading to 80,000 compounds left. Then, software DOCK4.0 [21] was employed, for constructing the grids for docking, residues within a radius of 3.5 Å around BMS309403 were used. The top 7800 compounds were then selected for the second round screening by GLIDE 4.0 [22,23] (www.schröinger.com). Receptor was prepared by using the Protein Preparation and Grid Preparation tools in the Schröinger Maestro interface. In the grid preparation process, the default settings were adopted for the cutoff, neutralization, scaling and dimensions of the binding pocket. The standard precision (SP) mode of GLIDE was used to explore the favorable binding poses. Ligand conformation is allowed to be flexible while the protein is held as a rigid structure during the docking process. After screening, 300 compounds with the highest scores were selected. Then these molecules were filtered by AUTODOCK3 program [24]. The center of the ligand BMS309403 was defined as the grid box center. The grid size was set to 40 × 40 × 40 points with grid spacing of 0.375 Å. The Lamarckian genetic algorithm was applied to account for protein–ligand interactions. According to the predicted binding conformations and their binding scores from GLIDE and AUTODOCK3, 199 compounds were purchased.

4.3. FABP4 inhibitory activity assays

The methods for expression, purification of FABP4 and the assay for FABP4 inhibition have been described in our previous studies [11,28]. The compounds were prepared as 100 mM stock solution in DMSO. Some of the compounds didn't dissolve well, then they were prepared in DMSO as 10 mM stock solution. On the day of activity assay, the compounds were all diluted in PBS to 100 μM for the first round activity test. Compounds that showed inhibition rate higher than 50% were selected for further IC$_{50}$ values determination.

4.4. Analysis of adipocyte lipolysis

The assay for evaluating the lipolysis of the compounds on 3T3-L1 adipocytes was described in our previous study [28]. Briefly, after mouse 3T3-L1 preadipocytes differentiated to adipocytes, the compounds or DMSO (final concentration 0.2%) with different concentrations were added to the 48-well plates for 24 h. On the day of experimentation, cells were incubated in Krebs Ringer Hepes buffer for 2 h, with or without 20 μM forskolin. Glycerol levels in supernatants were measured using a commercial Glycerol assay kit (Applygen Technologies Inc, China) for lipolysis determination.

4.5. Crystal structure determination

The purification and crystallization of human FABP4 was referred to the protocol of Eric Marr et al. [19] with slight modification. The cDNA of the full length FABP4 was cloned into pET28a vector with the Nde I/Xho I restriction sites. The recombinant protein was isolated by nickel-affinity chromatography, eluted with 50 mM NaH$_2$PO$_4$ pH8.0, 300 mM NaCl, 80 mM imidazole and then buffer exchanged into 20 mM HEPES pH7.5, 50 mM NaCl.

Crystals of FABP4 were obtained at 1.6 M Na-citrate at pH 6.5. Apo-FABP4 was soaked with 1 mM inhibitor in the reservoir solution overnight. Crystals were flash frozen in liquid nitrogen in the presence of well solution supplemented with 20% ethylene glycol (EG).

The Data sets were collected at 100 K on the beamline BL17U at the Shanghai Synchrotron Radiation Facility (SSRF), and were processed with the XDS software packages [29]. The structures were solved by molecular replacement, using the program PHASER [30] with the search model of PDB code 3P6C. The structures were refined using PHENIX [31]. Using the program Coot [32], inhibitor, water molecules were fitted into to the initial $F_o - F_c$ map. The refined structures were deposited to Protein Data Bank with accession codes 4NNS (FABP4-**9**) and 4NNT (FABP4-**10**). The complete statistics, as well as the quality of the solved structure, is shown in Table 3.

Table 3
Crystallographic data collection and refinement statistics.

PDB code	4NNS (FABP4-**9**)	4NNT (FABP4-**10**)
Space group	$P2_12_12_1$	$P2_12_12_1$
Cell dimensions: *a* (Å)	32.49	32.49
b (Å)	53.86	53.87
c (Å)	75.32	75.44
Wavelength (Å)	0.9793	0.9793
Reflections (unique)	19,991(1441)	20,579(1482)
Resolution range (Å)	1.53–43.81	1.53–29.84
Highest-resolution shell (Å)	1.53–1.57	1.53–1.57
Redundancy	5.14(5.36)	7.03(7.10)
$I/\sigma(I)$	27.95(9.73)	21.54(6.31)
Completeness (%)	96.9(96.7)	99.6(100)
R merge	4.3(21.5)	10.0(50.3)
R_{work}/R_{free} (%)	18.77/20.65	19.00/21.01
RMS values		
Bond length (Å)	0.005	0.006
Bond angle (°)	1.080	1.075
Number of non-hydrogen atoms		
Protein	1045	1034
Inhibitor	19	18
Water Oxygen	119	127
Others		
Mean temperature factors (Å^2)		
Protein	14.76	15.31
Inhibitor	14.80	15.10
Ramachandran plot		
Residues in most-favored regions	130(98.48%)	130(98.48%)
Residues in allowed regions	2(1.52%)	2(1.52%)
Residues in disallowed regions	0(0.00%)	0(0.00%)

4.6. The possible binding mode analysis of compound 4d using AUTODOCK4

The compound **4d** was docked by AUTODOCK4 program [24]. The center of the ligand **10** was defined as the grid box center. The grid size was set to 60 × 60 × 60 points with grid spacing of 0.375 Å. The docking parameters were set as follows: ga_pop_size = 150 (number of individuals in population), ga_run = 100 (the number of dockings that were performed), other parameters were set to the software's default values. The Lamarckian genetic algorithm was applied to account for protein–ligand interactions.

4.7. Statistical analysis

The IC_{50} value for compound against FABPs was determined by nonlinear regression using GraphPad Prism software (San Diego, CA, USA). Statistical significance of the data was performed using a one-way analysis of variance (ANOVA) followed by Dunnett's test. $p < 0.05$ is considered statistically significant.

Acknowledgments

This work was supported by grants from National Natural Science Foundation of China (81302699), the National Science and Technology Major Project "Key New Drug Creation and Manufacturing Program" (2012ZX09301-001-004), and the National 863 High Performance Computing Project (2012AA01A305).

References

[1] G.S. Hotamisligil, Inflammation and metabolic disorders, Nature 444 (7121) (2006) 860–867.
[2] A. Chmurzynska, The multigene family of fatty acid-binding proteins (FABPs): function, structure and polymorphism, J. Appl. Genet. 47 (1) (2006) 39–48.
[3] N.H. Haunerland, F. Spener, Fatty acid-binding proteins – insights from genetic manipulations, Prog. Lipid Res. 43 (4) (2004) 328–349.
[4] B.M. Spiegelman, M. Frank, H. Green, Molecular cloning of mRNA from 3T3 adipocytes. Regulation of mRNA content for glycerophosphate dehydrogenase and other differentiation-dependent proteins during adipocyte development, J. Biol. Chem. 258 (16) (1983) 10083–10089.
[5] C.R. Hunt, J.H. Ro, D.E. Dobson, H.Y. Min, B.M. Spiegelman, Adipocyte P2 gene: developmental expression and homology of 5′-flanking sequences among fat cell-specific genes, Proc. Natl. Acad. Sci. U. S. A. 83 (11) (1986) 3786–3790.
[6] G.S. Hotamisligil, R.S. Johnson, R.J. Distel, R. Ellis, V.E. Papaioannou, B.M. Spiegelman, Uncoupling of obesity from insulin resistance through a targeted mutation in aP2, the adipocyte fatty acid binding protein, Science 274 (5291) (1996) 1377–1379.
[7] K.T. Uysal, L. Scheja, S.M. Wiesbrock, S. Bonner-Weir, G.S. Hotamisligil, Improved glucose and lipid metabolism in genetically obese mice lacking aP2, Endocrinology 141 (9) (2000) 3388–3396.
[8] L. Makowski, J.B. Boord, K. Maeda, V.R. Babaev, K.T. Uysal, M.A. Morgan, R.A. Parker, J. Suttles, S. Fazio, G.S. Hotamisligil, et al., Lack of macrophage fatty-acid-binding protein aP2 protects mice deficient in apolipoprotein E against atherosclerosis, Nat. Med. 7 (6) (2001) 699–705.
[9] G. Tuncman, E. Erbay, X. Hom, I. De Vivo, H. Campos, E.B. Rimm, G.S. Hotamisligil, A genetic variant at the fatty acid-binding protein aP2 locus reduces the risk for hypertriglyceridemia, type 2 diabetes, and cardiovascular disease, Proc. Natl. Acad. Sci. U. S. A. 103 (18) (2006) 6970–6975.
[10] H. Lan, C.C. Cheng, T.J. Kowalski, L. Pang, L. Shan, C.C. Chuang, J. Jackson, A. Rojas-Triana, L. Bober, L. Liu, et al., Small-molecule inhibitors of FABP4/5 ameliorate dyslipidemia but not insulin resistance in mice with diet-induced obesity, J. Lipid Res. 52 (4) (2011) 646–656.
[11] H. Cai, G. Yan, X. Zhang, O. Gorbenko, H. Wang, W. Zhu, Discovery of highly selective inhibitors of human fatty acid binding protein 4 (FABP4) by virtual screening, Bioorg. Med. Chem. Lett. 20 (12) (2010) 3675–3679.
[12] A.V. Hertzel, K. Hellberg, J.M. Reynolds, A.C. Kruse, B.E. Juhlmann, A.J. Smith, M.A. Sanders, D.H. Ohlendorf, J. Suttles, D.A. Bernlohr, Identification and characterization of a small molecule inhibitor of fatty acid binding proteins, J. Med. Chem. 52 (19) (2009) 6024–6031.
[13] T. Barf, F. Lehmann, K. Hammer, S. Haile, E. Axen, C. Medina, J. Uppenberg, S. Svensson, L. Rondahl, T. Lundback, N-Benzyl-indolo carboxylic acids: design and synthesis of potent and selective adipocyte fatty-acid binding protein (A-FABP) inhibitors, Bioorg. Med. Chem. Lett. 19 (6) (2009) 1745–1748.
[14] R. Sulsky, D.R. Magnin, Y. Huang, L. Simpkins, P. Taunk, M. Patel, Y. Zhu, T.R. Stouch, D. Bassolino-Klimas, R. Parker, et al., Potent and selective biphenyl azole inhibitors of adipocyte fatty acid binding protein (aFABP), Bioorg. Med. Chem. Lett. 17 (12) (2007) 3511–3515.
[15] R. Ringom, E. Axen, J. Uppenberg, T. Lundback, L. Rondahl, T. Barf, Substituted benzylamino-6-(trifluoromethyl)pyrimidin-4(1H)-ones: a novel class of selective human A-FABP inhibitors, Bioorg. Med. Chem. Lett. 14 (17) (2004) 4449–4452.
[16] F. Lehmann, S. Haile, E. Axen, C. Medina, J. Uppenberg, S. Svensson, T. Lundback, L. Rondahl, T. Barf, Discovery of inhibitors of human adipocyte fatty acid-binding protein, a potential type 2 diabetes target, Bioorg. Med. Chem. Lett. 14 (17) (2004) 4445–4448.
[17] M.J. van Dongen, J. Uppenberg, S. Svensson, T. Lundback, T. Akerud, M. Wikstrom, J. Schultz, Structure-based screening as applied to human FABP4: a highly efficient alternative to HTS for hit generation, J. Am. Chem. Soc. 124 (40) (2002) 11874–11880.
[18] M. Furuhashi, G. Tuncman, C.Z. Görgün, L. Makowski, G. Atsumi, E. Vaillancourt, K. Kono, V.R. Babaev, S. Fazio, M.F. Linton, et al., Treatment of diabetes and atherosclerosis by inhibiting fatty-acid-binding protein aP2, Nature 447 (7147) (2007) 959–965.
[19] E. Marr, M. Tardie, M. Carty, T. Brown Phillips, I.K. Wang, W. Soeller, X. Qiu, G. Karam, Expression, purification, crystallization and structure of human adipocyte lipid-binding protein (aP2), Acta Crystallogr. Sect. F Struct. Biol. Cryst. Commun. 62 (Pt 11) (2006) 1058–1060.
[20] K. Hellberg, P.A. Grimsrud, A.C. Kruse, L.J. Banaszak, D.H. Ohlendorf, D.A. Bernlohr, X-ray crystallographic analysis of adipocyte fatty acid binding protein (aP2) modified with 4-hydroxy-2-nonenal, Protein Sci. 19 (8) (2010) 1480–1489.
[21] T.J.A. Ewing, I.D. Kuntz, Critical Evaluation of Search Algorithms for Automated Molecular Docking and Database Screening, 1997.
[22] R.A. Friesner, J.L. Banks, R.B. Murphy, T.A. Halgren, J.J. Klicic, D.T. Mainz, M.P. Repasky, E.H. Knoll, M. Shelley, J.K. Perry, et al., Glide: a new approach for rapid, accurate docking and scoring. 1. Method and assessment of docking accuracy, J. Med. Chem. 47 (7) (2004) 1739–1749.
[23] Glide: A New Approach for Rapid, Accurate Docking and Scoring. 2. Enrichment Factors in Database Screening.
[24] G.M. Morris, D.S. Goodsell, R.S. Halliday, R. Huey, W.E. Hart, R.K. Belew, A.J. Olson, Automated docking using a Lamarckian genetic algorithm and an empirical binding free energy function, J. Comput. Chem. 19 (14) (1998) 1639–1662.
[25] B. Binas, H. Danneberg, J. McWhir, L. Mullins, A.J. Clark, Requirement for the heart-type fatty acid binding protein in cardiac fatty acid utilization, FASEB J. 13 (1999) 805–812.
[26] K. Maeda, H. Cao, K. Kono, C.Z. Gorgun, M. Furuhashi, K.T. Uysal, Q. Cao, G. Atsumi, H. Malone, B. Krishnan, Y. Minokoshi, B.B. Kahn, R.A. Parker, G.S. Hotamisligil, Adipocyte/macrophage fatty acid binding proteins control integrated metabolic responses in obesity and diabetes, Cell Metab. 1 (2005) 107–119.

[27] N.R. Coe, M.A. Simpson, D.A. Bernlohr, Targeted disruption of the adipocyte lipid-binding protein (aP2 protein) gene impairs fat cell lipolysis and increases cellular fatty acid levels, J. Lipid. Res. 40 (1999) 967–972.
[28] H.Y. Cai, T. Wang, J.C. Zhao, P. Sun, G.R. Yan, H.P. Ding, Y.X. Li, H.Y. Wang, W.L. Zhu, K.X. Chen, Benzbromarone, an old uricosuric drug, inhibits human fatty acid binding protein 4 in vitro and lowers the blood glucose level in db/db mice, Acta Pharmacol Sin. 34 (11) (2013) 1397–1402.
[29] W. Kabsch, XDS, Acta Crystallogr. D66 (2010a) 125–132.
[30] A.J. McCoy, R.W. Grosse-Kunstleve, P.D. Adams, M.D. Winn, L.C. Storoni, R.J. Read, Phaser crystallographic software, J. Appl. Crystallogr. 40 (Pt 4) (2007) 658–674.
[31] P.D. Adams, P.V. Afonine, G. Bunkoczi, V.B. Chen, I.W. Davis, N. Echols, J.J. Headd, L.W. Hung, G.J. Kapral, R.W. Grosse-Kunstleve, et al., PHENIX: a comprehensive Python-based system for macromolecular structure solution, Acta Crystallogr. D Biol. Crystallogr. 66 (Pt 2) (2010) 213–221.
[32] P. Emsley, B. Lohkamp, W.G. Scott, K. Cowtan, Features and development of Coot, Acta Crystallogr. D Biol. Crystallogr. 66 (Pt 4) (2010) 486–501.